How to reveal metastable skyrmionic spin structures by spin-polarized scanning tunneling microscopy

New Journal of Physics
The open access journal at the forefront of physics

Deutsche Physikalische Gesellschaft DPG
IOP Institute of Physics

Published in partnership with: Deutsche Physikalische Gesellschaft and the Institute of Physics

OPEN ACCESS

RECEIVED
30 November 2015

REVISED
11 April 2016

ACCEPTED FOR PUBLICATION
6 May 2016

PUBLISHED
26 May 2016

PAPER

How to reveal metastable skyrmionic spin structures by spin-polarized scanning tunneling microscopy

B Dupé[1], C N Kruse, T Dornheim and S Heinze

Institute of Theoretical Physics and Astrophysics, Christian-Albrechts-Universität zu Kiel, D-24098 Kiel, Germany
[1] Author to whom any correspondence should be addressed.

E-mail: dupe@theo-physik.uni-kiel.de

Keywords: spin polarized STM, Monte Carlo simulation, density functional theory

Abstract

We predict the occurrence of metastable skyrmionic spin structures such as antiskyrmions and higher-order skyrmions in ultra-thin transition-metal films at surfaces using Monte Carlo simulations based on a spin Hamiltonian parametrized from density functional theory calculations. We show that such spin structures will appear with a similar contrast in spin-polarized scanning tunneling microscopy images. Both skyrmions and antiskyrmions display a circular shape for out-of-plane magnetized tips and a two-lobe butterfly contrast for in-plane tips. An unambiguous distinction can be achieved by rotating the tip magnetization direction without requiring the information of all components of the magnetization.

1. Introduction

Magnetic skyrmions were recently observed via neutron diffraction in bulk chiral magnets such as MnSi [1] and in the multiferroic material Cu_2OSeO_3 [2]. Currently, they are attracting an enormous attention due to their stability [3, 4] and their displacement speed upon applying electrical currents, which makes them suitable for technological applications [5, 6]. Real space observation of skyrmions in FeGe and $Fe_{0.5}Co_{0.5}Si$ thin films has become possible using Lorentz microscopy and magnetic force microscopy [7–10], and more recently, in transition-metal films using spin-polarized low-energy electron microscopy [11] and magneto-optical Kerr effect measurements [12]. In ultra-thin films of a few monolayers, the skyrmion diameter can shrink down to a few nanometers and spin-polarized scanning tunneling microscopy (SP-STM) [13, 14] is a powerful tool for their observation and manipulation [15–17].

SP-STM is sensitive to the projection of the local magnetization density of states of the sample onto the magnetization direction of the tip [18] and does not allow a direct determination of the three magnetization components in a single measurement. Additionally, in most experimental setups it is not possible to continuously rotate the tip magnetization direction and conclusions have to be drawn from SP-STM experiments performed with only one or two tip magnetization directions. Such measurements only allow a partial determination of the spin structure [16, 19, 20]. It is therefore essential (i) to know if the skyrmion ground states and some metastable states can be differentiated via simple SP-STM experiments (based on one or two tip magnetization directions) and (ii) to establish a clear proposal in order to discriminate between the different possible chiral spin structures via SP-STM.

2. Methods

The occurrence of metastable skyrmionic spin structures is studied in a single atomic layer of Pd in fcc stacking on the fcc monolayer Fe on the Ir(111) surface denoted as Pd(fcc)/Fe/Ir(111). This system has been studied experimentally using SP-STM [16, 17] and from first-principles calculations [21, 22] which allow to understand the transition from a spin spiral to a skyrmion and a ferromagnetic (FM) phase in an external magnetic field. We numerically solve the spin Hamiltonian using Monte-Carlo (MC) simulations with parameters obtained from

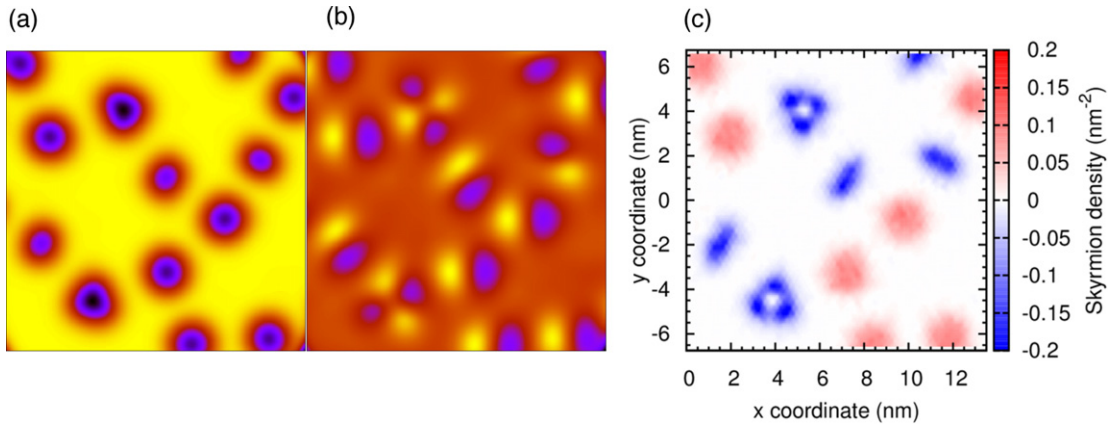

Figure 1. Simulated SP-STM image with an out-of-plane (a) and an in-plane (b) magnetized tip at $z = 8$ Å from the surface for a spin structures of 13×13 nm^2 obtained from MC simulations for Pd(fcc)/Fe/Ir(111). (c) Skyrmion density of the spin structure (color contrast). The spin structure was obtained with a super cell of 100×100 spins on a hexagonal lattice at a temperature of 1 K after a relaxation with 10^7 MC relaxation starting from a random spin configuration at a magnetic field of $B = 20$ T, i.e. in the region of the phase diagram in which the ferromagnetic state is the ground state.

density functional theory calculations [21]:

$$H = -\sum_{ij} J_{ij}\mathbf{M}_i \cdot \mathbf{M}_j - \sum_{ij}\mathbf{D}_{ij} \cdot (\mathbf{M}_i \times \mathbf{M}_j) + \sum_i K\,(M_i^z)^2 + \sum_i \mathbf{B} \cdot \mathbf{M}_i \quad (1)$$

with exchange constants J_{ij}, the vector $\mathbf{D}_{ij}$ of the Dzyaloshinskii–Moriya interaction, the magnetocrystalline anisotropy K and an external magnetic field[2].

We obtained metastable states in MC simulations by relaxing a super cell of 100×100 spins on a two-dimensional hexagonal lattice starting from a random spin configuration at 1 K under a magnetic field of 20 T with a standard Metropolis algorithm. At this field value we are in the region where the skyrmions are metastable in the FM background [21].

We simulated SP-STM images of the spin structures obtained from MC using the model described in [23]. The tunneling current is given by

$$I(\mathbf{R}_T) \propto \sum_\alpha (1 + P_T P_S \cos\theta_\alpha)\, h(\mathbf{R}_T - \mathbf{R}_\alpha), \quad (2)$$

where $\mathbf{R}_T$ is the tip position, the sum extends over all surface atoms α, the vacuum tail of a spherical atomic wave function is approximated by $h(\mathbf{r}) = \exp(-2\kappa|\mathbf{r}|)$, and the decay constant is given by $\kappa = \sqrt{2m\phi/\hbar^2}$ with the work function ϕ. P_S and P_T denote the spin-polarization of sample and tip atoms, respectively, and θ_α is the angle of the magnetization of atom α with respect to the tip magnetization direction $\mathbf{m}_T$.

3. Results

Figure 1(a) shows a simulated SP-STM image with an out-of-plane magnetized tip ($P_{\text{eff}} = P_T P_S = 0.4$) of the spin structure at $z = 8$ Å from the surface. The image shows a brighter contrast for the FM background with several black spots. All darker spots have a round shape and might correspond to skyrmion spin structures. However, when the tip magnetization is changed from out-of-plane to in-plane (figure 1(b)), the simulated SP-STM image shows two types of contrast compatible with recent observations of skyrmions [17]. The first contrast has a two-lobe pattern with one brighter and one darker side. The lobes can be aligned along the x-axis or are rotated by 60° or 120° with respect to it. The second type of contrast has four lobes and appears seldom. It does not seem to have a preferred alignment.

[2] We have obtained the coefficients of the spin Hamiltonian from first-principles calculations for Pd(fcc)/Fe/Ir(111) [21]. The exchange constants J_n between the nth nearest-neighbors in the Fe layer $J_1 \cdots J_{10}$ are given, in meV, by 14.73, −1.95, −2.88, 0.32, 0.69, 0.01, 0.01, 0.13, −0.14, −0.28, respectively, the anisotropy constant is $K = -0.7$ meV, which corresponds to an out-of-plane easy axis and the DMI constant is $D = 1.0$ meV.

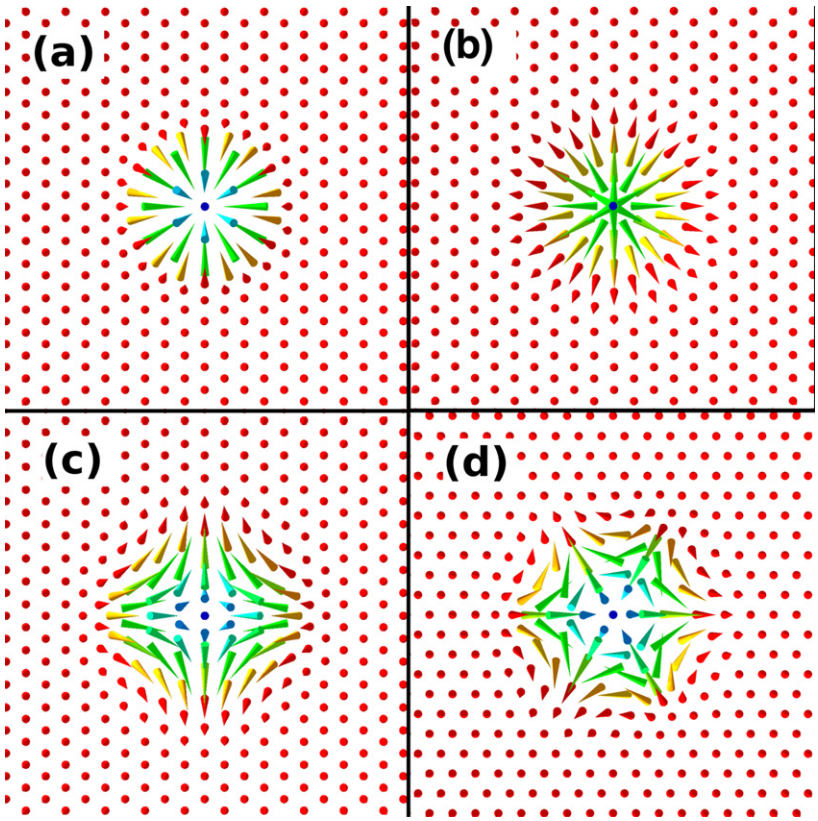

Figure 2. Metastable chiral spin textures relaxed at $T = 0$ K and $B = 20$ T for Pd(fcc)/Fe/Ir(111). (a) Right-handed skyrmion ($S = 1$). (b) Left-handed skyrmion ($S = 1$). (c) Antiskyrmion ($S = -1$). (d) Higher-order antiskyrmion ($S = -2$). Depending on the angle θ of the magnetic moment with respect to the z-axis perpendicular to the film, the color of the arrows changes from red for $\theta = 0$ (or $\mathbf{m}$ pointing upwards) to blue for $\theta = \pi$ (or $\mathbf{m}$ pointing downwards). Green arrows ($\theta = \pi/2$) correspond to in-plane spins.

The topological character of different spin structures is given by their winding or skyrmion number:

$$S = \frac{1}{4\pi} \int \mathbf{m} \cdot \left(\frac{\partial \mathbf{m}}{\partial x} \times \frac{\partial \mathbf{m}}{\partial y} \right) \mathrm{d}x\mathrm{d}y, \tag{3}$$

where $\mathbf{m}$ is the unit vector of the local magnetization and S can take only integer values. Figure 1(c) shows the skyrmion density as expressed by the integrand of equation (3) as a color contrast. This quantity can differentiate the different spin structures but is not accessible in experiments. The two-lobe patterns correspond to a skyrmion (red contrast), which has a positive skyrmion density that integrates to $S = 1$, or to an anti-skyrmion with a negative skyrmion density ($S = -1$) (blue contrast). The four-lobe contrast has a triangular shaped skyrmion density that integrates to the value of $S = -2$ suggesting the presence of a metastable higher order anti-skyrmion in this system. Experimentally, the different spin structures can be obtained by freezing an ultra-thin film sample from high temperatures to a very low temperature e.g. 1 K under magnetic field or by locally heating the sample [24] e.g. with an electrical current while maintaining it at low temperature.

In order to compare the different states in detail, we show in figure 2 the distinct spin structures identified in figure 1 in separate panels. Figure 2(a) shows a right-handed skyrmion i.e. $S = 1$ which is metastable for Pd(fcc)/Fe/Ir(111) at magnetic field values higher than 16 T [21]. For completeness, we also consider a left-handed skyrmion, figure 2(b), which has a skyrmion number of $S = 1$ as well but exhibits an opposite chirality and is unstable in this system. Figure 2(c) shows an antiskyrmion ($S = -1$) that is characterized by a change of chirality for two high symmetry directions, i.e. the rotational sense changes from right- to left-handed every 90°. Figure 2(d) displays the higher-order antiskyrmion with $S = -2$, which was recently also reported in [25]. In that case, the rotational sense changes every 60°.

The simulated STM images of the isolated spin structures are shown in figure 3. An out-of-plane magnetized tip (left column of figure 3) is sensitive to the perpendicular component of the local magnetization direction. For the FM background, the tunneling current is high which creates the yellow contrast. The current decreases when the tip scans across the skyrmion due to the antiparallel spin alignment and the contrast darkens. All spin structures appear as spherical entities in this imaging mode. When the tip magnetization changes to in-plane, the images of the right-handed skyrmion (figure 3(b)), the left-handed skyrmion (figure 3(d)) and the antiskyrmion

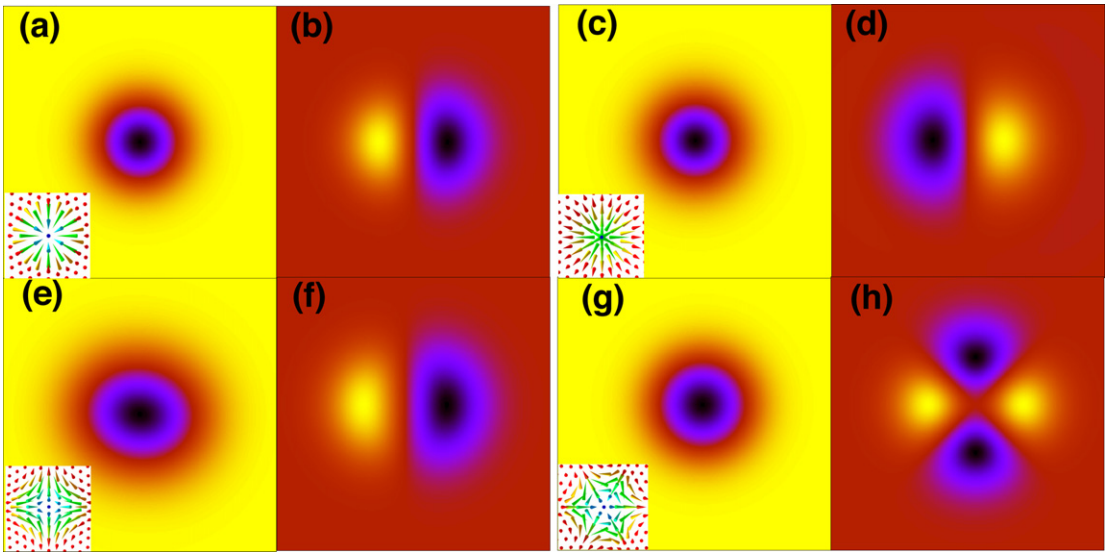

Figure 3. Simulated SP-STM images for an out-of-plane magnetized tip (a, c, e, g) and for an in-plane magnetized tip along the horizontal axis (b, d, f, h). (a) and (b) right-handed skyrmion, (c) and (d) left-handed skyrmion, (e) and (f) antiskyrmion, (g) and (h) higher-order antiskyrmion. For all spin structures the image area as well as the color scale of the contrast are the same. The insets show the spin structures.

(figure 3(f)) are still very similar. The simulated SP-STM images of a skyrmion and an antiskyrmion could only differ by a rotation with respect to the magnetization direction of the tip as seen in figure 1(b). The only spin structure that can be easily distinguished is the higher-order skyrmion due to the multiple nodes of the contrast with the in-plane magnetized tip (see figure 3(h)). Note, that the simulated SP-STM images of the right-handed skyrmion for both magnetization directions are in good agreement with the experiments of Romming *et al* [16, 17].

The contrast of the SP-STM images can be quantified by the corrugation amplitude, i.e. the maximal change of tip height as it is scanned across the spin structure, which is obtained by analyzing scan lines. From the simulated images one expects that such line profiles are very similar, which is indeed confirmed in figure 4. For an out-of-plane magnetized tip, which leads to qualitatively very similar contrasts in the SP-STM images (see figure 3), we obtain line profiles which are also in quantitative agreement with experimental data [17]. These line profiles are characterized by a smooth change from a high tip-sample separation in the FM background (when the magnetization of the tip and the local magnetization of the sample are aligned) to a low separation at the center of the spin structures. We found corrugation amplitudes in the same order of magnitude in our simulations for all spin structures, with corrugation values of 5.6, 4.4, 6.4, and 7.1 pm for the right-handed skyrmion, the left-handed skyrmion, the antiskyrmion and the higher-order antiskyrmion, respectively. These corrugation amplitudes are on the same order as found in experiments [17].

When the tip magnetization is switched to in-plane, the line profiles show the same behavior for the right-handed skyrmion, the left-handed skyrmion and the antiskyrmion (figures 4(a)–(c)). Since the contrast of the SP-STM images of the skyrmion and antiskyrmion are only rotated with respect to each other and the corrugation amplitudes are very similar, they can only be distinguished in experiments when both spin structures are present simultaneously. On the other hand, the higher-order skyrmion (figure 4(d)) can be easily discriminated due to the presence of multiple nodes of the magnetization density also seen in figure 3(h).

In order to distinguish between the skyrmion and the antiskyrmion spin structures, we propose an experiment based on a 3D vector field available in STM experiments [26]. Such a field enables a rotation of the tip magnetization both within the surface plane as well as from in-plane to out-of-plane. Although all in-plane magnetized tips result in the same contrast i.e. a butterfly with a bright and a dark lobe (as shown in figure 3), the behavior of this contrast when the tip changes its direction is different as shown in figure 5. For a right-handed skyrmion, the lobes will rotate in phase with the tip magnetization direction (thick black arrows). In the case of an antiskyrmion, a clockwise rotation of the in-plane component of the tip will induce a counterclockwise rotation of the lobes. Therefore, in-plane rotation of the tip magnetization allows an unambiguous distinction between the right-handed skyrmion and the antiskyrmion. On the other hand, in order to distinguish a left- and right-handed skyrmion the tip magnetization must be rotated from the in-plane to the out-of-plane direction.

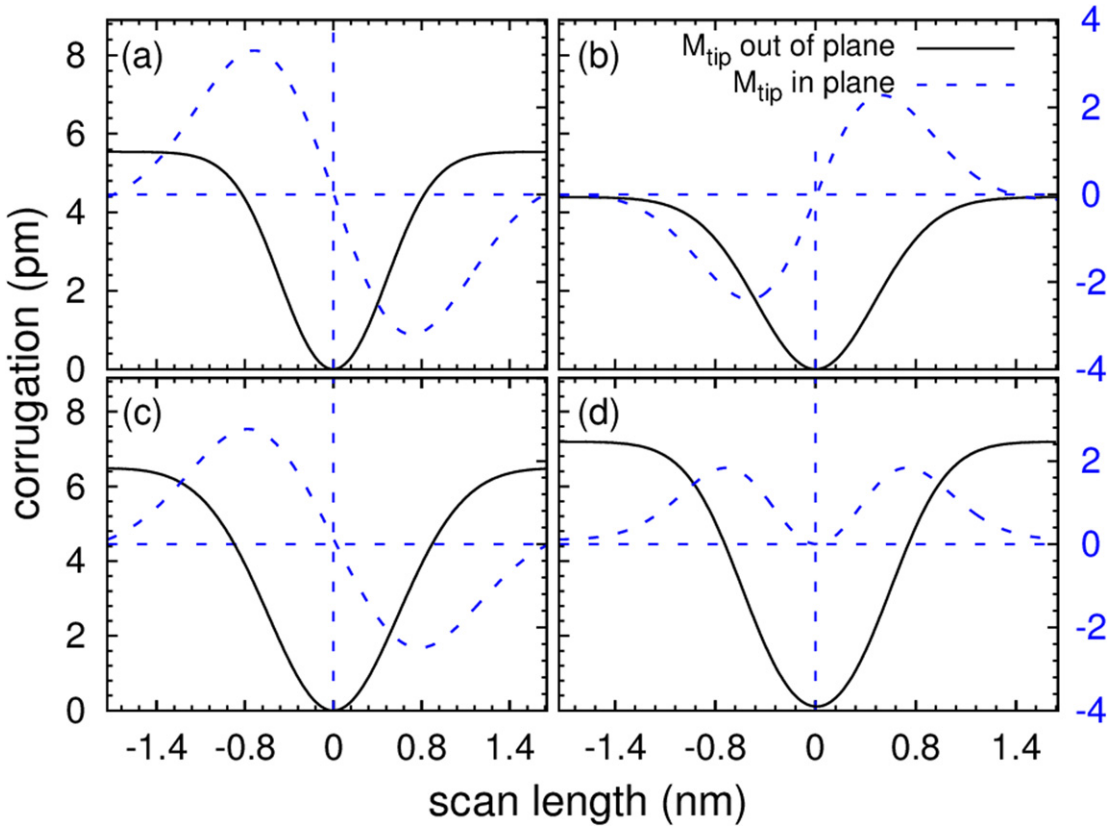

Figure 4. Line profiles of the simulated SP-STM images for the topologically different spin structures of figure 3. Solid black lines correspond to an out-of-plane magnetized tip and dashed blue lines correspond to an in-plane magnetized tip. Line profile of (a) the right-handed skyrmion, (b) the left-handed skyrmion, (c) the antiskyrmion and (d) the higher-order antiskyrmion.

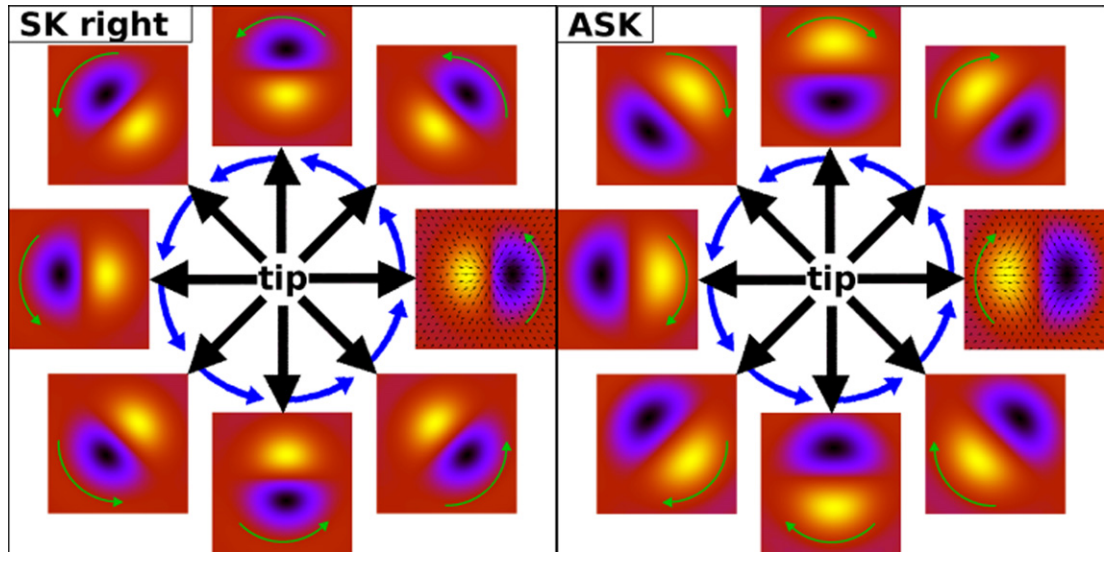

Figure 5. Simulated SP-STM experiments in which the tip magnetization is rotated in the film plane. For a right-handed skyrmion (left panel), the butterfly contrast rotates clockwise as the magnetization of the tip is rotated clockwise, while for an antiskyrmion (right panel), the butterfly rotates counterclockwise opposite to the tip magnetization.

4. Conclusion

In conclusion, we have demonstrated that it is non-trivial to distinguish via SP-STM between metastable spin structures at surfaces that differ by their chirality and/or topological charge. Skyrmions and antiskyrmions exhibit a spherical shape in SP-STM using tips with an out-of-plane magnetization. For in-plane magnetized tips

we obtain a characteristic butterfly pattern that is aligned along the tip magnetization for skyrmions, while the alignment depends on the antiskyrmion orientation with respect to the tip magnetization. If the tip magnetization is rotated within the surface plane the butterfly contrast rotates in phase with the tip direction for skyrmions and in the opposite direction for antiskyrmions allowing to unambiguously distinguish between them. The demonstration of stabilizing localized spin structures with different chirality and topological charge in the same system e.g. Pd/Fe/Ir(111), opens new possibilities for spintronics [27].

Acknowledgments

B Dupé and S Heinze thank the Deutsche Forschungsgemeinschaft (DFG) for financial support via the project DU 1489/2-1 and gratefully acknowledge computing time at the HLRN supercomputer. This project has received funding from the European Unions Horizon 2020 research and innovation programme under grant agreement No. 665095 (FET -Open project MAGicSky).

References

[1] Mühlbauer S, Binz B, Jonietz F, Pfleiderer C, Rosch A, Neubauer A, Georgii R and Böni P 2009 *Science* **323** 915–9
[2] Seki S, Yu X Z, Ishiwata S and Tokura Y 2012 *Science* **336** 198–201
[3] Bogdanov A and Hubert A 1994 *Phys. Status Solidi* b **186** 527–43
[4] Bogdanov A and Hubert A 1994 *J. Magn. Magn. Mater.* **138** 255–69
[5] Fert A, Cros V and Sampaio J 2013 *Nat. Nanotechnol.* **8** 152–6
[6] Nagaosa N and Tokura Y 2013 *Nat. Nanotechnol.* **8** 899–911
[7] Yu X, Onose Y, Kanazawa N, Park J, Han J, Matsui Y, Nagaosa N and Tokura Y 2010 *Nature* **465** 901–4
[8] Yu X Z, Kanazawa N, Onose Y, Kimoto K, Zhang W Z, Ishiwata S, Matsui Y and Tokura Y 2010 *Nat. Mater.* **10** 106
[9] Huang S X and Chien C L 2012 *Phys. Rev. Lett.* **108** 267201
[10] Milde P *et al* 2013 *Science* **340** 1076
[11] Chen G, Mascaraque A and Schmid A K 2015 *Appl. Phys. Lett.* **106** 242404
[12] Jiang W *et al* 2015 *Science* **349** 283
[13] Bode M 2003 *Rep. Prog. Phys.* **66** 523
[14] Wiesendanger R 2009 *Rev. Mod. Phys.* **81** 1495–550
[15] Heinze S, von Bergmann K, Menzel M, Brede J, Kubetzka A, Wiesendanger R, Bihlmayer G and Blügel S 2011 *Nat. Phys.* **7** 713–9
[16] Romming N, Hanneken C, Menzel M, Bickel J E, Wolter B, von Bergmann K, Kubetzka A and Wiesendanger R 2013 *Science* **341** 636–9
[17] Romming N, Kubetzka A, Hanneken C, von Bergmann K and Wiesendanger R 2015 *Phys. Rev. Lett.* **114** 177203
[18] Wortmann D, Heinze S, Kurz P, Bihlmayer G and Blügel S 2001 *Phys. Rev. Lett.* **86** 4132–5
[19] von Bergmann K, Kubetzka A, Pietzsch O and Wiesendanger R 2014 *J. Phys.: Condens. Matter.* **26** 394002
[20] Phark S H, Fischer J A, Corbetta M, Sander D, Nakamura K and Kirschner J 2014 *Nat. Commun.* **5** 5183
[21] Dupé B, Hoffmann M, Paillard C and Heinze S 2014 *Nat. Commun.* **5** 4030
[22] Simon E, Palotás K, Rózsa L, Udvardi L and Szunyogh L 2014 *Phys. Rev.* B **90** 094410
[23] Heinze S 2006 *Appl. Phys.* A **85** 407–14
[24] Koshibae W and Nagaosa N 2014 *Nat. Commun.* **5** 5148
[25] Leonov A O and Mostovoy M 2015 *Nat. Commun.* **6** 8275
[26] Meckler S, Mikuszeit N, Preßler A, Vedmedenko E Y, Pietzsch O and Wiesendanger R 2009 *Phys. Rev. Lett.* **103** 157201
[27] Koshibae W and Nagaosa N 2016 *Nat. Commun.* **7** 10542